

Original Research

MAXIMUM POWER EXTRACTION USING TWISTING SLIDING MODE CONTROLLER FOR WIND ENERGY SYSTEMS

Asaad Abed Faisal*, Turki Kahawish Hassan

Electrical Engineering Department, College of Engineering, Mustansiriyah University, Baghdad, Iraq

Received 18/06/2022

Accepted in revised form 22/10/2022

Published 01/07/2023

Abstract: This paper presents a systematic control scheme for a wind energy conversion system with variable speed and describes a permanent magnet synchronous generator PMSG with five phases. The machine employs back-to-back converters, while the grid-side converters are used. Stator current and mechanical rotation speed control are employed to accomplish maximum power point tracking operation on the machine side converter at wind speed below the rated speed. The pitch of the angle is used to limit the extracted wind energy when the wind surpasses the specified wind. The grid current control loop regulates both active and reactive power injection at the unity power factor for the grid side converter. The five-phase PMSG rotor speed is controlled by the twisting sliding mode controller in order to maintain the reference speed in various wind speeds. Performance comparisons between the twisting sliding mode controller, conventional proportional integral controller, and integral sliding mode controller show that the twisting sliding mode controller is superior to the other controllers in steady state error. According to this study, the overall efficiency is increased to 94% when using the TSMC controller rather than the ISMC and PI controllers, which are currently at 92.45% and 88.12% respectively. MATLAB/Simulink simulation results are used to verify the effectiveness of the suggested control technique.

Keywords: *Phase locked loop; total harmonics distortion; machine side converter; grid side converter; twisting sliding mode control.*

1. Introduction

Wind power is a promising direction for electricity generation. The use of renewable

clean wind energy helps to cover the increasing electricity consumption of a growing world population as demonstrated in [1-3]. Because of wind energy conversion systems (WECS) maximize power extraction energy and increase efficiency over fixed-speed systems. The methods for developing and running them have drawn a lot of interest as in [4]. In variable-speed wind turbine systems (VS-WTS), the doubly-fed induction generator (DFIG) as in [5] or (PMSG) as in [6] is commonly used. The PMSG recently has seen a significant increase in use due to of own excellent characteristics of simple structure, effective energy outcome, gear reduction building, self-excitation, and low noise as demonstrated in [7]. Three-phase generators provide electricity. According to recent research, multi-phase machines, such as five-phase machines, increase performance in renewable energy, aerospace, oil and gas, and hybrid and electric autos. Five-phase technology benefits many generators and motors, especially those that need softer, smaller, more convenient, and reliable power production systems. Our method improves torque ripple, capacitor needs, power density, and fault tolerance, based on manufacturing methods that have been tried and

*Corresponding Author:

eema2006@uomustansiriyah.edu.iq

Work of This Research is
Licensed under CC BY



tested, as illustrated in [8,9]. The three-phase dual machine as given in [10] as well as the six-phase machine shown in [11] are two multi-phase topologies used by WECS. Multiphase generators do give more degrees of freedom for fault-tolerant operation. The five-phase PMSG is widely employed in a variety of applications, including the Marine Current Turbine (MCT), and the remaining healthy phases of the PMSG can be used to recompense for faults and keep the MCT running as demonstrated in [12,13]. Furthermore, the development of huge power electronic devices aids in the improvement of controllability and reliability as in [14]. Power electronics converter topologies are coupled to the power grid to increase WECS quality and reliability as illustrated in [15]. Putri et al. in [16] present control of the model on the generator and grid sides by using two control strategies. Due to the unpredictability and increased intermittency of wind power production, wind power producers must be incorporated into the grid, which is problematic. As a consequence, effective synchronization approaches are required as shown in [17, 18]. Several studies investigated maximum power point tracking (MPPT) and blade pitch control in WECS as illustrated in [19–21]. Janaszek et al. in [22] and Hosseyni et al. in [23] proposed numerous multiphase machine control approaches that have been developed, including multiphase direct torque control (DTC) and field orientation control (FOC). More than just building the controller, system control architecture is a multi-stage process. Before making a controller, a design goal needs to know enough about the system wants to control. Traditional vector control architectures for multiphase machine-driven applications, such as proportional-integral (PI) controllers, have several limitations, including parameter tuning difficulties, inferior dynamic performance, and lower resilience as in [24,25]. The sliding mode

control (SMC) is an excellent control technique for dealing with PI controller weak resilience and static and dynamic performance, has a basic structure and idea, and is resistant to system uncertainties and unknown disruptions, solar electricity uses SMC as demonstrated in [26-28], wind turbine systems as given in [29-31] and additional applications are being added every day. Shtessel et al. in [32] described the primary motivation for developing second-order sliding mode control (SOSMC) is to minimize chattering. Despite their ability to effectively reduce and change chattering, alternative (SOSMC) methods, such as twisting sliding mode controller (TSMC), suboptimal algorithms, control algorithms with preset convergence criterion, and quasi-continuous control algorithms. The structure of the paper is summarized below: The analytical modeling of the WECS consists of WT model and the five-phase PMSG is presented in Section 2. Section 3 describes the control system, which includes the GSC and MSC, as well as the suggested TSMC controller and the MPPT approach for pitch angle management. Section 4 presented the simulation results, comments, and the dynamic response of the system are in. Finally, section 5 contains the conclusion.

2. Modeling of WECS

A structure consisting of a wind turbine (WT), a generator, and a VSMT. To measure the maximum wind output, use a PWM rectifier on the generator. The WECS model presented in Fig. 1 also includes a grid-side PWM inverter to regulate active and reactive power on the grid independently [14].

2.1. Model of the Wind Turbine

The power of the air stream is the flow of kinetic energy per unit of time through the cross-

sectional area of the turbine rotor blade as illustrated in [6, 28]:

$$P_w = 0.5 \rho A V_w^3 \tag{1}$$

the mechanical power developed by the turbine can be expressed as:

$$P_m = 0.5 \rho A C_p(\lambda, \beta) V_w^3 \tag{2}$$

Where C_p stands for the power coefficient, which is equal to (P_m/P_w) , ρ is the air density, $(A = \pi R^2)$, A an area swept by the wind turbine rotor, R is the blade length of the turbine, λ is the tip speed ratio (TSR), β is the pitch angle and V_w is the wind speed.

The C_p can be modeled by the following equation

$$C_p(\lambda, \beta) = 0.5176 \left(\frac{116}{\lambda_i} - 0.4\beta - 5 \right) \exp(-21/\lambda_i) + 0.0068\lambda \tag{3}$$

$$\frac{1}{\lambda_i} = \frac{1}{\lambda + 0.08\beta} - \frac{0.35}{1 + \beta^3} \tag{4}$$

$$\lambda = \frac{\omega_r}{V_w} R \tag{5}$$

ω_r is the turbine rotational speed, The mechanical torque T_m of the turbine can be obtained as follows:

$$T_m = \frac{P_m}{\omega_r} \tag{6}$$

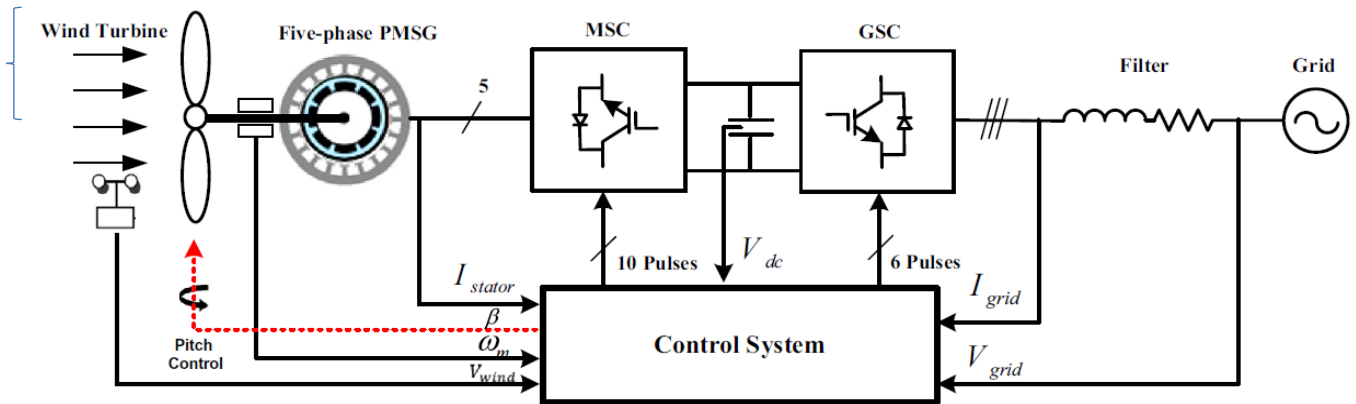


Figure 1. Configuration of a WECS [21]

Fig. 2 represents the relationship between the C_p and λ . The optimal value of C_p and λ are equal to 0.48 and 8.1 respectively, can be obtained only when β is equal to zero as in [33]. Fig. 3 illustrates the power delivered by the wind turbine plotted as a function of the rotational speed of the wind turbine for different wind speeds.

According to the graphs, wind speed an effect on the MPP. The TSR must be maintained at the optimal operating position for every given wind speed to maximize power generation as given in [33-34].

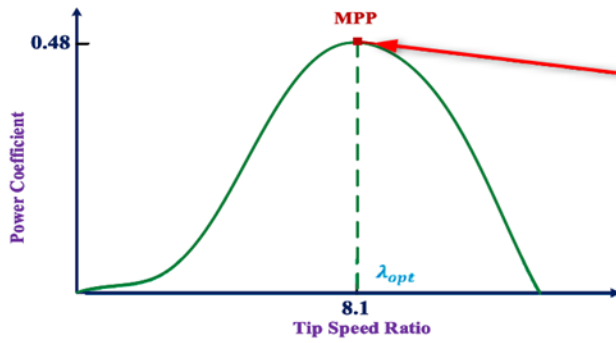


Figure 2. Relation between C_p and λ [33]

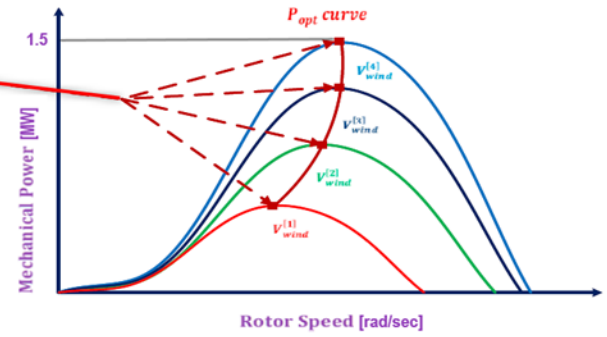


Figure 3. Relation between P_m and ω_r [33]

2.2. Dynamic Model for Five Phases of PMSG

The d and q-axis stator voltage components in the synchronous rotating frame can be described using Park's Transformation on the five-coordinate of the PMSG dynamic model as [13,35]:

$$\begin{cases} V_{d1} = R_s i_{d1} + L_{d1} \frac{di_{d1}}{dt} - \omega_e L_q i_{q1} \\ V_{q1} = R_s i_{q1} + L_{q1} \frac{di_{q1}}{dt} + \omega_e L_d i_{d1} + \omega_e \psi_{pm} \\ V_{d2} = R_s i_{d2} + L_{d2} \frac{di_{d2}}{dt} - 3 \omega_e L_q i_{q2} \\ V_{q2} = R_s i_{q2} + L_{q2} \frac{di_{q2}}{dt} + 3 \omega_e L_d i_{d2} \end{cases} \quad (7)$$

Where R_s is the stator resistance, $L_{d,q}$ is the stator dq-axis inductance, $V_{d1,d2}$ and $V_{q1,q2}$ the dq-axis voltage of the stator, $i_{d1,d2}$ and $i_{q1,q2}$ dq-axis current of the stator, ω_e is the electrical angular velocity and ψ_{pm} is the rotor permanent magnet flux-linkage.

when the air gap in the PMSG is uniform, then the $L_d = L_q = L_s$. The electromagnetic torque of 5-phase PMSG can be represented by forcing the current components (i_{d1} , i_{d2} and i_{q2}) to zero.

$$T_e = 2.5 p \psi_{pm} i_{q1} \quad (8)$$

For a wind turbine system, the mechanical equation is as follows:

$$\omega_m = \frac{1}{J} (T_m - T_e - B \omega_m) \quad (9)$$

Where B denotes the friction coefficient and J the moment of inertia.

3. Control System

3.1. Machine Side Control

Fig. 4 shows the (MSC), which contains a wind turbine directly connected with a five-phase PMSG that is connected with the grid at unity power factor via BTBC. The control scheme contains two internal and external control loops. The external loop control is used to control the rotational speed while the internal control loop is used to control the current. The control loop of the speed uses a TSMC type controller to control the speed and creates an i_{q1} reference current component generated during wind speed changes on which the electromagnetic torque T_e depends according to equation (8). Furthermore, by reducing the other current components (i_{d1} , i_{d2} and i_{q3}) to zero, the internal control loop is employed to manage the constant current components d-q, ensuring that the maximum torque per ampere is obtained, as demonstrated in [7,20,23]. Current control is accomplished by using on/off hysteresis switching. The proposed control (TSMC) is used to treat and improve the performance and response of the dynamic system and improve efficiency in addition, the steady-

state error is almost negligible, in contrast to the used control PI and ISMC, which suffers from

a poor forced response and steady-state error, In addition to the overshooting in the ISMC controller as in [4,25].

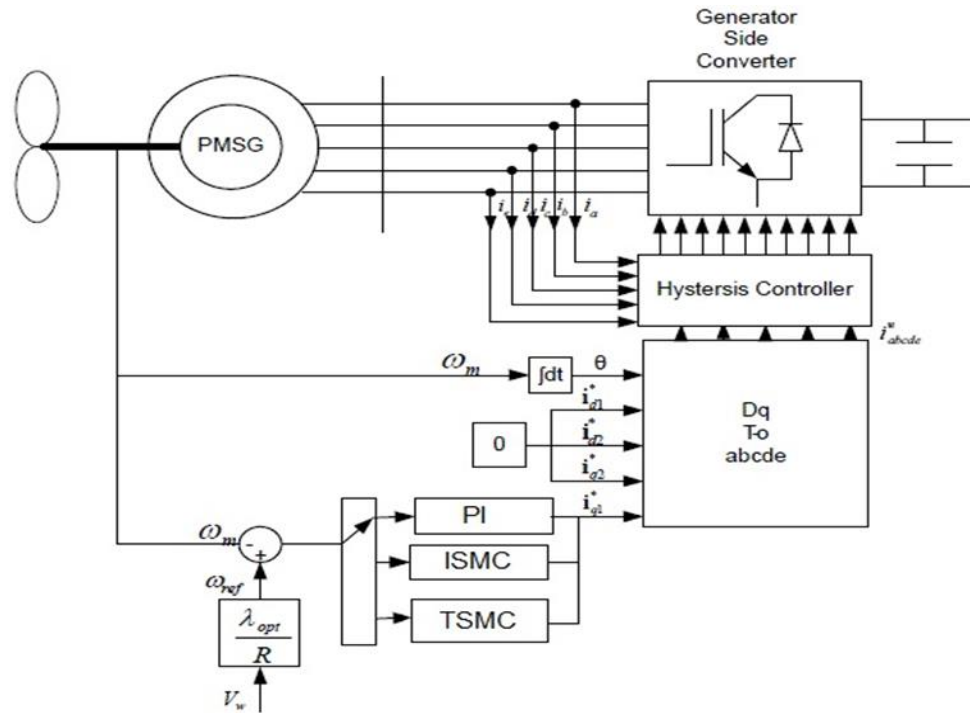


Figure 4. Machine side control (MSC)

3.1.1. MPPT Technique

To create the reference speed command, an MPPT controller is utilized. This instruction will allow the WECS to harvest the highest amount of power possible from the available wind power. Furthermore, for any instantaneous wind speed, the ideal rotational speed of the wind turbine rotor may be calculated using the following formula as shown in [7,20]:

$$\omega_{ref} = \frac{\lambda_{opt} \cdot V_w}{R} \tag{10}$$

The reference speed is compared with the actual speed of the five-phase PMSG and the error from the difference between them is applied to the proposed controller as in [20]. The maximum power point follows a path that is proportional to

the cubic of the wind speed as demonstrated in [34].

$$P_{m-max} = 0.5 \rho A C_{pmax} \left[\frac{R \cdot \omega_{ref}}{\lambda_{opt}} \right]^3 \tag{11}$$

The goal of a good wind generator controller is to change the output current of the generator to reach the speed that provides the maximum power for each wind speed. This can of course only be done if you have a variable speed generator.

3.1.2. Regulation of pitch angle

Regulation systems that change the pitch angle of the blade, also known as variable pitch, have the capability of rotating the blades along their longitudinal axis to adjust the power based on wind conditions, increasing the rotor's aerodynamic efficiency. This technology

provides for the extraction of nominal electrical power at wind speeds greater than the nominal. As well as a high-speed wind security mechanism. The pitch servo motor is powered by the gain as shown in Fig. 5.

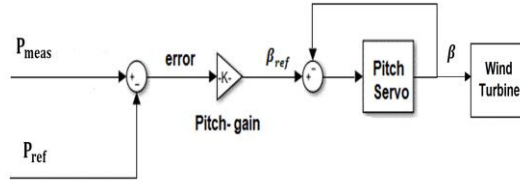


Figure 5. Pitch angle Control

3.1.3. Twisting sliding mode control (TSMC)

Because power electronic systems are prone to nonlinearities, such as uncertainties, unmolded dynamics, and disturbance. As a result, SMC is employed in power electronic systems due to features like high robustness against system uncertainties, unknown disturbances, fast response, complete controllability, flexibility, high control performance, high efficiency, simple structure, and concept. The proposed TSMC avoids the chattering in the control action and minimized the steady state error in the traditional PI controller and ISMC controller. In SOSMC both the sliding surface (*s*) and the state error variable (*e*) converge to zero in a finite time. In order to design the TSMC, two steps must be taken. The sliding surface must first be made and the second is to get the controller function *U_c* as illustrated in [31,32].

The twisting algorithm is defined by the following equation given in [32]:

$$U_c = U_{eq} + U_{un} \tag{12}$$

Where *U_c* is the controller function, *U_{eq}* is a linear (continuous part, equivalent control) and the *U_{un}* which is a nonlinear (discontinuous part). Sliding surface can be defined as:

$$S_\omega = e_\omega \tag{13}$$

Where *e_ω* is the difference speed and is equal to (*e_ω* = *ω_{ref}* - *ω_m*).

$$\dot{S}_\omega = \dot{e}_\omega = \dot{\omega}_{ref} - \dot{\omega}_m \tag{14}$$

By substituting eq. (8) and eq. (9) into eq. (14) yield:

$$\dot{S}_\omega = \dot{\omega}_{ref} - \frac{1}{J} (T_m - 2.5 p \psi_{pm} i_{q1} - B \omega_m) \tag{15}$$

Arranging (15),

$$\dot{S}_\omega = \underbrace{\dot{\omega}_{ref}}_{\phi} - \underbrace{\frac{1}{J} (T_m - B \omega_m)}_{m(t)} + \underbrace{\frac{2.5 p \psi_{pm}}{J} i_{q1}}_{\gamma} \tag{16}$$

$$\dot{S}_\omega = \phi + \gamma U_c - m(t) \tag{17}$$

Where *m(t)* represents all system disturbances.

The control component can be calculated as

$$\ddot{S}_\omega = \dot{S}_\omega = m(t) = 0 \tag{18}$$

$$0 = \phi + \gamma U_{eq} \implies U_{eq} = \frac{-\phi}{\gamma} \tag{19}$$

As a result, the controller function to ensure a reachability condition can be rewritten as:

$$\begin{cases} U_c = U_{eq} + U_{un} \\ = -\gamma^{-1} (\phi + r_1 \operatorname{sgn}(s) + r_2 \operatorname{sgn}(\dot{s})) \\ r_1 > r_2 > 0 \end{cases} \tag{20}$$

The sat function is used instead of signum function to decrease the chattering issue, as well as add two terms to solve the problem of the reaching phase instability. The *K_s* and *K_ω* are selected to provide the highest performance while minimizing dynamic system disturbances.

$$\left\{ \begin{array}{l} U_c = U_{eq} + U_{un} \\ = -\gamma^{-1} (\emptyset + r_1 \text{sat}(s) + r_2 \text{sat}(\dot{s}) + K_s S_\omega + \\ K_\omega \omega_m) \quad r_1 > r_2 > 0 \end{array} \right. \quad (21)$$

3.2. Control of the Grid Side

The fundamental objective of the GSC is to provide active power to the grid at a power factor of one and use the method of voltage-oriented control to regulate the DC-link voltage Fig.6. There is two loop control in the GSC, the first loop is the outer control utilized to maintain a constant DC-link voltage at reference value, and the second loop is an inner control that regulates the dq-axis current in order to give active power to the grid at all times (UPF) as demonstrated in [4,7,33]. The inverter can be supplied with frequency and phase angle by utilizing a phase-locked loop (PLL). The objective is to synchronize the inverter's current angle with the grid's voltage angle to achieve a power factor as

close to (UPF) as feasible as in [36]. In a reference frame rotating synchronously with the grid voltage, the dynamic model of the grid connection is as follows [34]:

$$V_{gd} = V_{id} - RI_{gd} - L \frac{d}{dt} I_{gd} + L \omega_g I_{gq} \quad (22)$$

$$V_{gq} = V_{iq} - RI_{gq} - L \frac{d}{dt} I_{gq} - L \omega_g I_{gd} \quad (23)$$

where L is the grid inductance and R is the grid resistance.

V_{id} and V_{iq} are the d-q axis inverter voltage components. The $V_{gq} = 0$, As a result, the power system is only supplied with active power as shown in [21]. the grid vector voltage is:

$$V = V_{gd} + j0 \quad (24)$$

The following equations are used to express active and reactive power:

$$P_g = \frac{3}{2} V_{gd} I_{gd} \quad (25)$$

$$Q_g = \frac{3}{2} V_{gd} I_{gq} \quad (26)$$

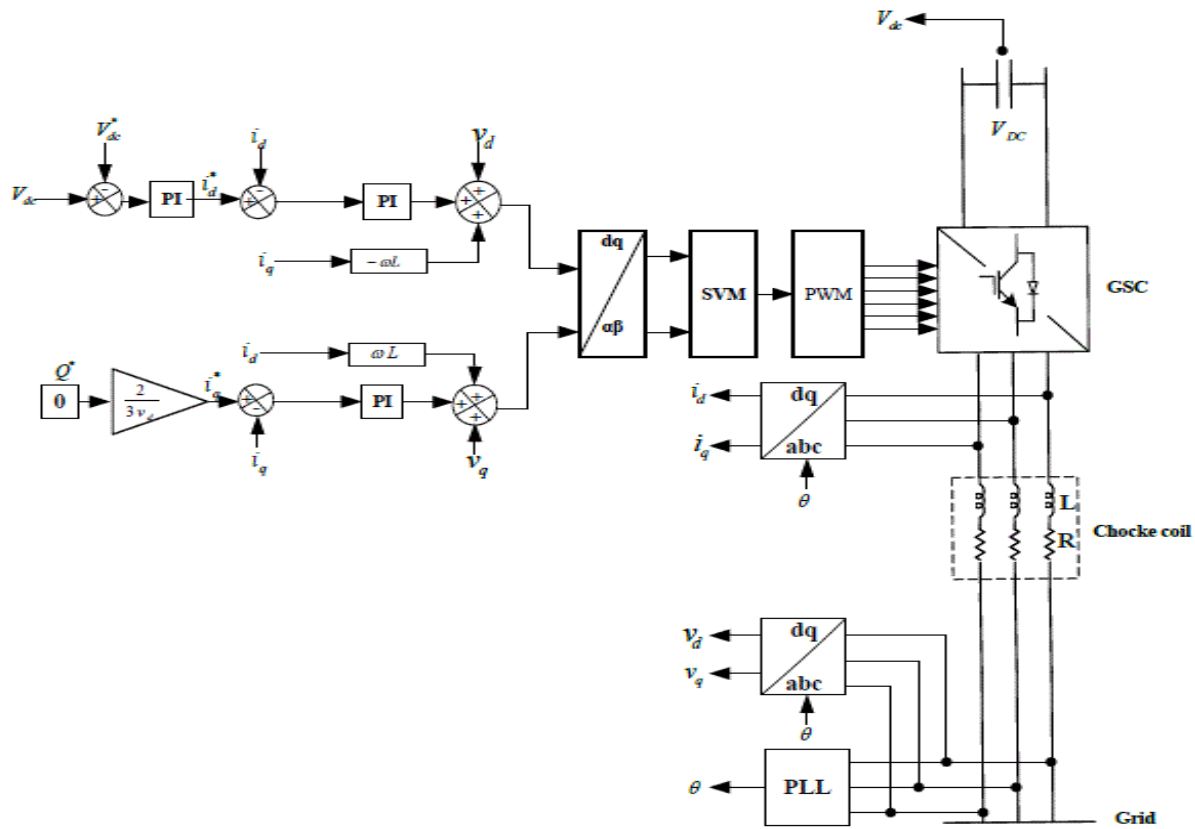


Figure 6. Grid side control [34].

4. Results of the Simulation and Discussion

The system under study is based on a 5-phase PMSG linked to the grid through BTBC and developed in MATLAB/Simulink R2020a. The suggested TSMC is implemented at different wind speeds, as well as the MPPT and the angle of the blade angle control in the MSC controller. The DC-link capacitor voltage and current management are controlled by the GSC controller. The Ziegler-Nichols approach is used to get the best PI controller gain value. All the system parameters, including ISMC, TSMC, and PI gains, have been chosen to ensure the system will work well as shown in appendices I and II. Fig.7 to Fig. 10 illustrate the WT characteristics. Fig. 7 shows the variable wind speed as a step function with a period from zero to 20 seconds

where the wind speed at 5 seconds changed to 12m/s, at 10 seconds changed to 13m/s, and at 15 seconds changed to 11m/s. The pitch angle is displayed in Fig. 8, where we can see that at speeds under the specified wind speed the angle β is zero degrees, while at speeds above the rated wind speed, the pitch angle is roughly 1.745 degrees at 13m/s as stated in Table 1.

Table 1. Features of wind turbines

V_{wind} (m/s)	C_p	λ	β (degree)	ω_{ref} (rad/sec)
10	0.48	8.1	0	2.642
11	0.48	8.1	0	2.908
12	0.48	8.1	0	3.171
13	0.3789	7.476	1.745	3.171
14	0.3019	6.939	5.688	3.171
15	0.2457	6.477	9.89	3.171

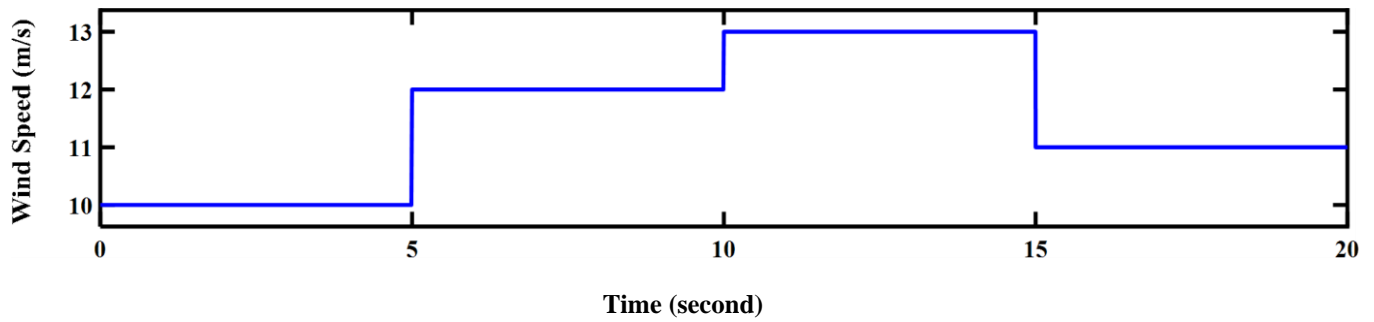


Figure 7. Variation of wind speed

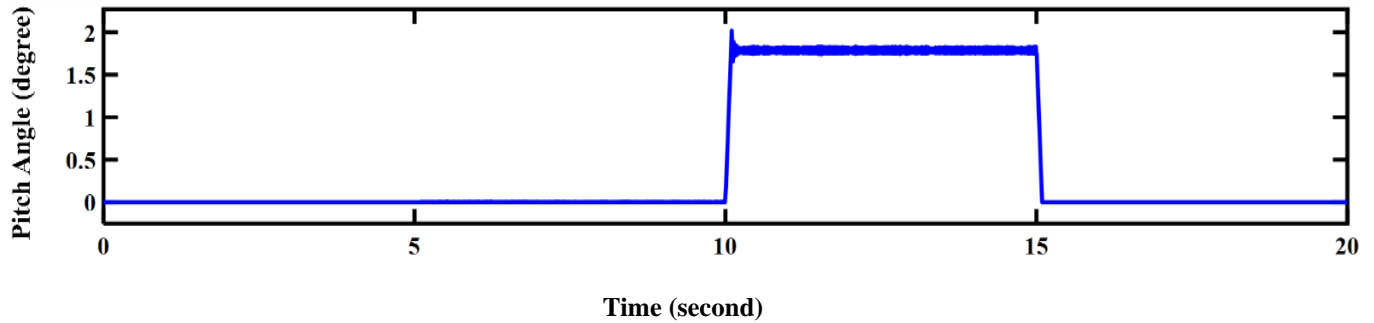


Figure 8. Pitch angle (β) at variable wind speed

Fig. 9(a, b) shows the tip speed ratio (TSR) at different ways of controlling, where using PI and ISMC controllers in Fig. 9(a) and TSMC controller in Fig. 9(b) yet obvious that the TSR is constant at value 8.1 at speeds underrated speed and start to decrease under 8.1 to 7.476 at 13m/s, 6.939 at 14m/s, 6.477 at 15m/s when speed exceeded the rated wind speed 12m/s Table 1.

Fig. 10(a, b) illustrate the power coefficient (C_p) also at different methods of controlling such as Fig. 8, the C_p values when the speed less than the specified wind speed is constant at 0.48, while starting to decrease at speed below rated wind speed.

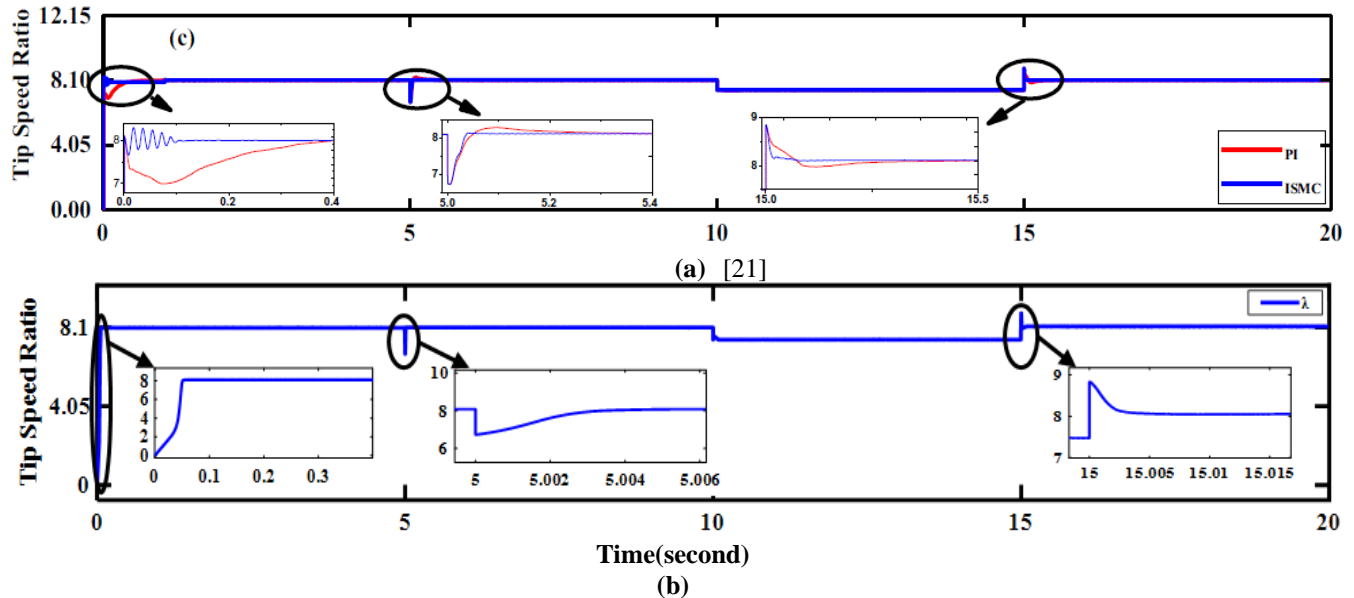


Figure 9. Tip Speed Ratio (λ) [(a) PI, ISMC controllers and (b) TSMC controller]

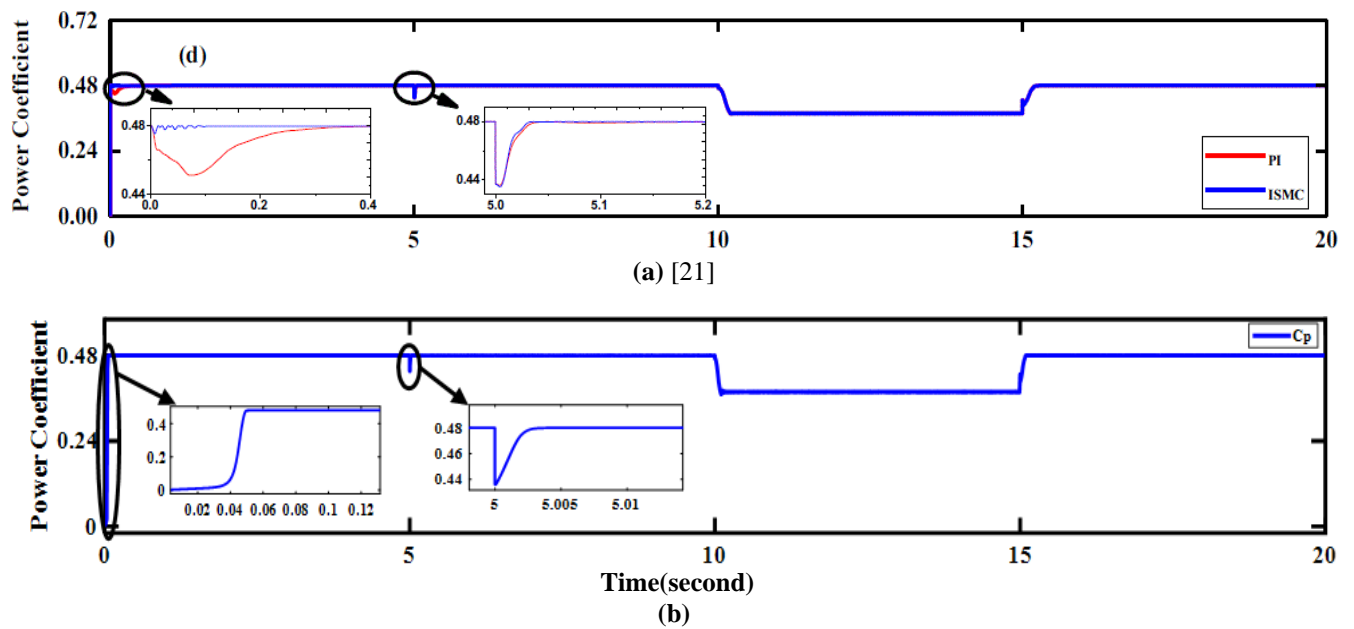


Figure 10. Power coefficient (C_p) [(a) PI, ISMC, and (b) TSMC]

The generator side characteristics represented in Fig. 11 to Fig. 14 demonstrate how speed controllers affect rotor speed and mechanical power. Fig.11(a, b) shows the reference and actual rotor speed which can be tracked by using PI, ISMC, and TSMC, noted that the settling time is 0.005 second in TSMC while is 0.705 seconds and 0.112 second in conventional PI and ISMC respectively at a rated wind speed 12 m/s [21]. Fig. 12(a, b) illustrates the actual and reference

mechanical power. shows that the TSMC has the best performance over the PI and ISMC controllers. Fig. 13 shows the match between the electromagnetic torque and mechanical torque because of the direct drive between the WT and 5-phase PMSG. Fig. 14 shows the five-phase current where note that the waveform is a pure sinusoidal waveform, in addition there are change in current under variation of wind speed.

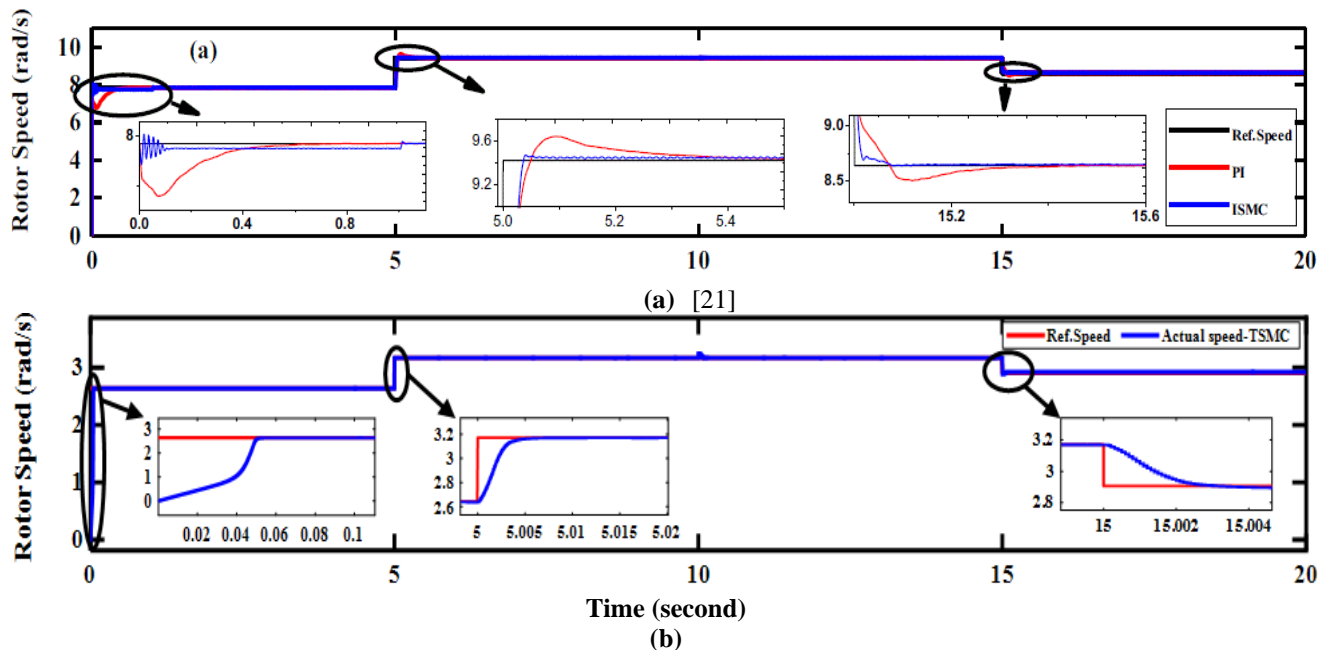


Figure 11. Rotor Speed [(a) PI, ISMC and (b) TSMC]

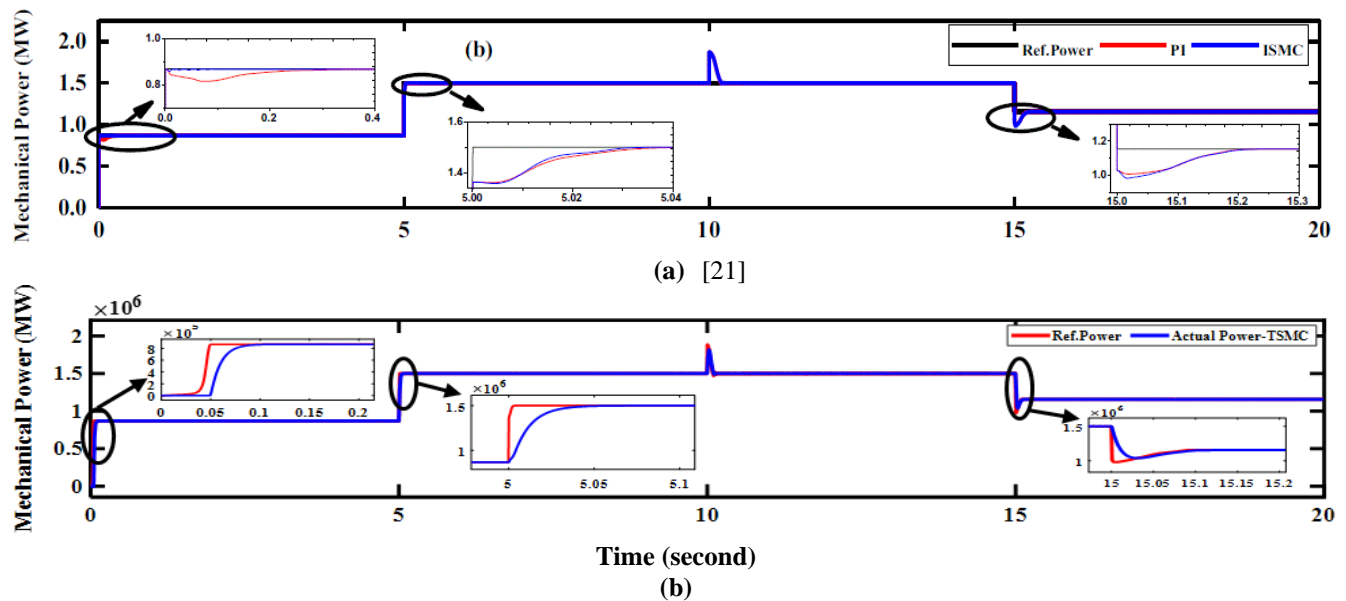


Figure 12. Mechanical Power [(a) PI, ISMC and (b) TSMC]

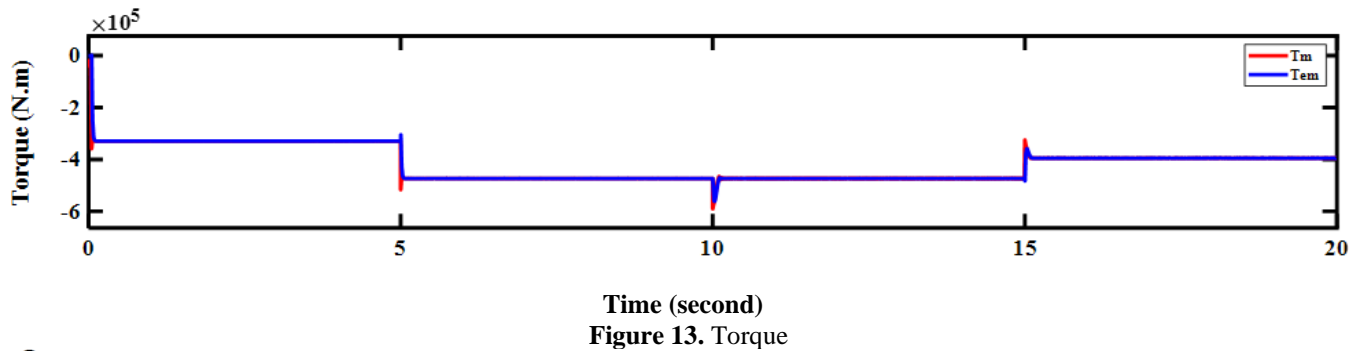


Figure 13. Torque

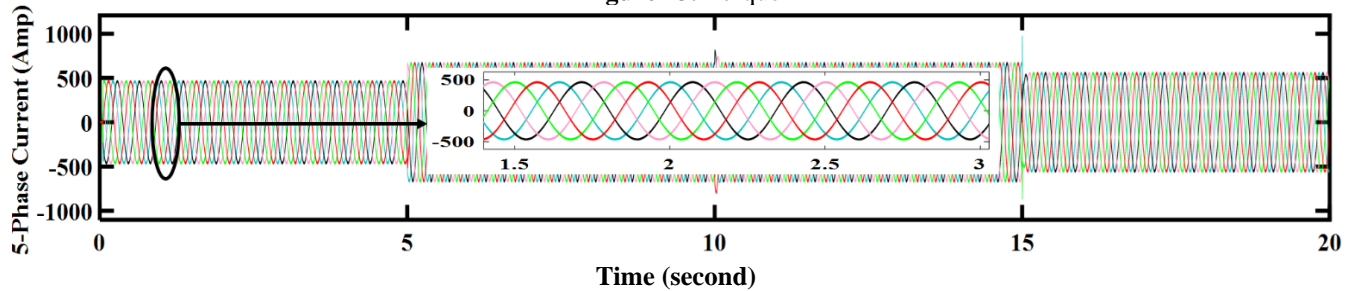


Figure 14. Five Phase Current

Fig. 15 to Fig. 19 show the properties of the GSC. Despite variations in wind speed, the DC-link voltage remains constant at 1150 V Fig. 15. Fig. 16 shows the phase voltage and current, clear that the voltage and current are in the same phase at a frequency of 60 Hz, and the amplitude of phase current is about 2000 A. Fig.17 illustrates the real power injected into the grid at UPF with the value

of 1.41 MW at a rated wind speed of 12m/s and reactive power around zero value to guarantee UPF Fig. 18. Fig. 19 represents the THD% with a minimum value of about 1.953% for TSMC and 2.19%, 2.35 for the ISMC and PI controllers respectively. This is as a result of the proposed controller.

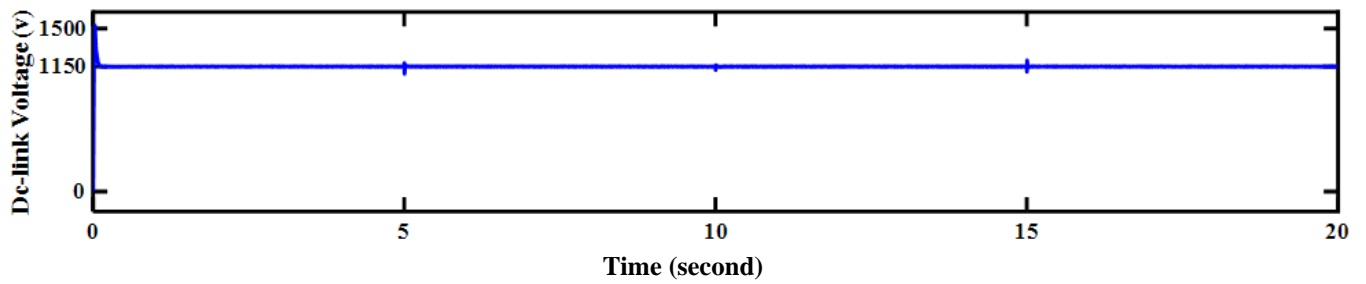


Figure 15. DC-link Voltage

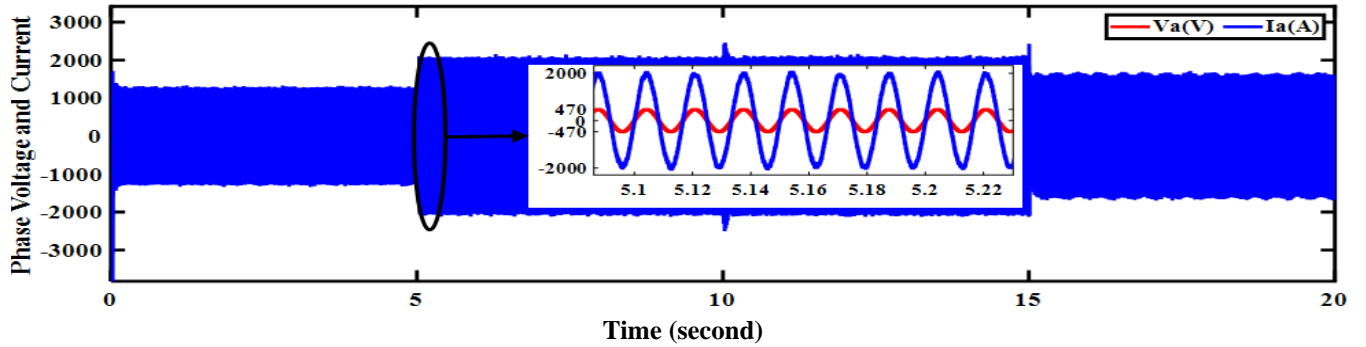


Figure 16. Phase Voltage and Current

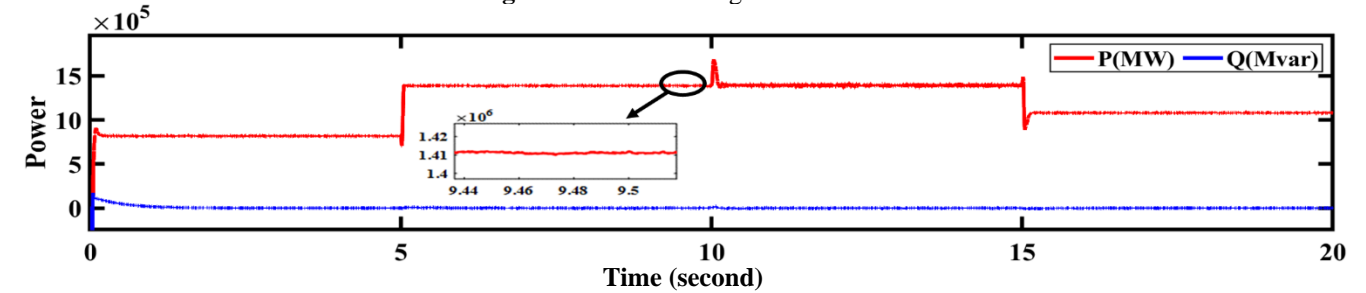


Figure 17. Active and Reactive Power

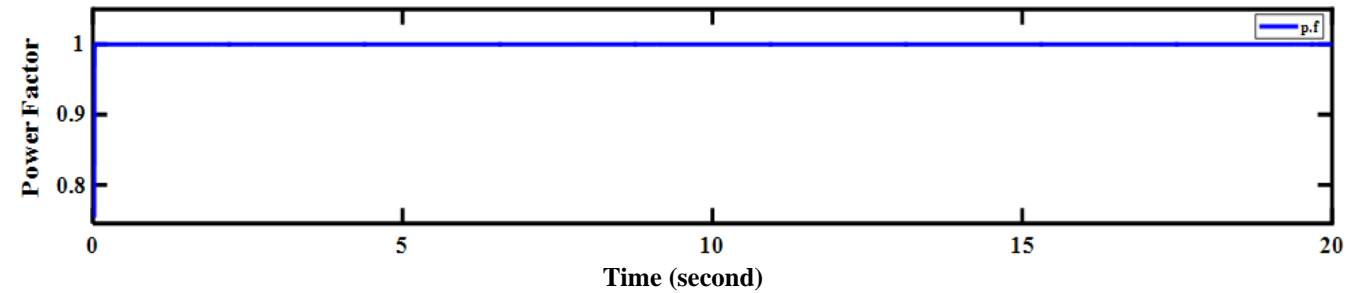


Figure 18. Power Factor

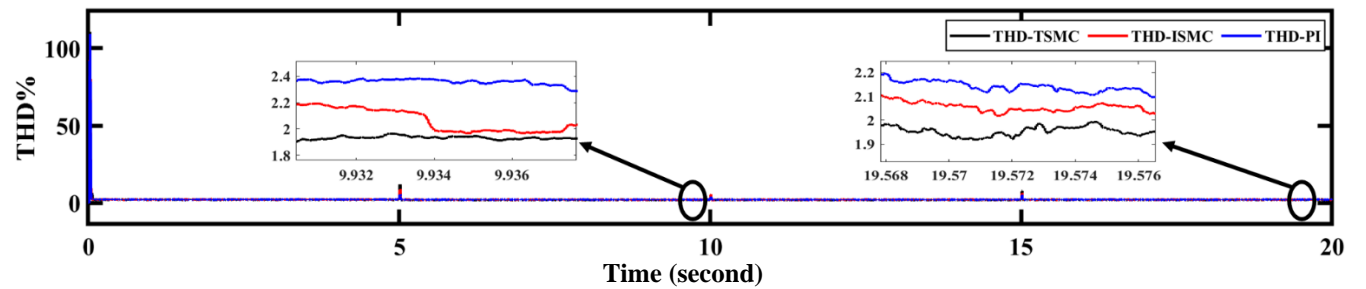


Figure 19. Total Harmonics Distortion%

The suggested TSMC controller provides excellent control and performance in terms of

speed regulation [25]. The dynamic response of the TSMC, PI, and ISMC controllers is shown in

Fig. 11(a, b). The settling time of the TSMC is 4 msec, while the settling times of the ISMC and PI controllers are 112 msec and 705 msec, respectively. The overshoot and undershoot in the TSMC controller are negligible, in contrast to the PI and ISMC controllers which have overshoot and undershoot. Clear that the reference speed is varied to 2.642 at 10m/s, 2.908 at 11m/s below rated wind speed, and remained Constant to 3.171(rad/s) at all speeds over rated wind speed 12m/s because of the pitching angle Table 1. The main goal of the controllers is to increase energy capture and ensure operating at a safety zone at or underrated wind speed. A comparison of theoretical power and real grid power is done to validate the efficiency of the proposed WECS-based control systems [33]:

$$\eta_{sys} = \frac{P_g}{P_{th}} \times 100\% \quad (27)$$

where η_{sys} indicates WECS efficiency, P_g refers to grid-injected power, and P_{th} refers to theoretical extracted power that can be evaluated from eq. (1). Table 2 lists the performance characteristics such as steady-state error, settling time response, and overall system efficiency, which reveal that the TSMC performs better in terms of overall system performance. The proposed TSMC boosts total system efficiency by 94%, compared to 92.45% for the ISMC and 88.12% for the PI controller Table 2.

Table 2. A comparative analysis of the TSMC, traditional PI, and ISMC for WECS over a long period.

Controller	Steady-state error (percentage%)	Settling time (msec.)	η_{sys} (%)
Conventional PI	0.841	705	88.12%
ISMC	0.204	112	92.45%
TSMC	0.031	5	94%

5. Conclusions

This research offers a more accurate TSMC controller in comparison to the classic PI and ISMC controllers. Demonstrates that the TSMC surpasses the traditional PI and ISMC controllers in terms of performance. The proposed TSMC speed controller improves the system's steady-state error and dynamic response, the settling time is 0.005 second for TSMC and 0.112 second and 0.705 second for the ISMC and PI controllers respectively. Furthermore, the steady-state error is 0.031% for TSMC and 0.204%, and 0.841% for the ISMC and PI controllers respectively. The overshoot and downshoot are low in comparison to the PI and ISMC controllers. The total harmonics distortion reduced to 1.953% due to suggested control while 2.19% and 2.35% for ISMC and PI controllers respectively. Due to using the proposed TSMC, the overall WECS efficiency reached 94% compared with ISMC and PI controllers is 92.45% and 88.12% respectively. Extensive simulations using MATLAB and SIMULINK are utilized to evaluate the suggested control approach with varying wind speed profiles. In terms of dynamic performance, the simulation results indicate that the TSMC outperforms the competition in the advanced control system that enables to manage rotor speed in a range of conditions.

Acknowledgments

The authors would like to express their gratitude to the Iraqi Ministry of Higher Education and Scientific Research and the College of Engineering, Electrical Engineering Department at Mustansiriyah University for their scientific assistance and support.

Conflict of interest

There is no conflict of interest in the current project.

Author Contribution Statement

All authors contributed to the writing and editing of this manuscript. Author Turki K. Hassan proposed the research problem and supervised the findings of this work. Author Asaad A. Faisal suggests a control method to improve system performance. Both authors discuss the results and contributed to the final manuscript.

References

- Jenkins, N., Burton, T., Bossanyi, E., Sharpe, D., & Graham, M. (2021). *Wind Energy Handbook 3e*. Wiley. ISBN:9781119451143.
<https://doi.org/10.1002/9781119451143>
- Kaldellis, J. K., & Apostolou, D. (2017). *Life cycle energy and carbon footprint of offshore wind energy Comparison with onshore counterpart*. *Renewable Energy*, Vol.108, August 2017, pp. 72-84.
<https://doi.org/10.1016/j.renene.2017.02.039>
- Hossain, M. M., & Ali, Mohd. H. (2015). *Future research directions for the wind turbine generator system*. *Renewable and Sustainable Energy Reviews*. Vol. 49, September 2015, pp. 481-489.
<https://doi.org/10.1016/j.rser.2015.04.126>
- Moutchou, R., & Abbou, A. (2019). *Comparative Study of SMC and PI Control of a Permanent Magnet Synchronous Generator Decoupled by Singular Perturbations*. 2019 7th International Renewable and Sustainable Energy Conference (IRSEC), 2019, pp. 1-7,
<https://doi.org/10.1016/j.rser.2015.04.12610.1109/IRSEC48032.2019.9078310>
- Yang, B., Zhang, X., Yu, T., Shu, H., & Fang, Z. (2017). *Grouped grey wolf optimizer for maximum power point tracking of doubly-fed induction generator-based wind turbine*. *Energy Conversion and Management*, Vol. 133, 1 February 2017, pp. 427-443.
<https://doi.org/10.1016/j.enconman.2016.10.062>
- Xie, D., Lu, Y., Sun, J., & Gu, C. (2017). *Small signal stability analysis for different types of PMSGs connected to the grid*. *Renewable Energy*, Vol. 106, June 2017, pp. 149-164.
<https://doi.org/10.1016/j.renene.2017.01.021>
- Tripathi, S. M., Tiwari, A. N., & Singh, D. (2015). *Grid-integrated permanent magnet synchronous generator-based wind energy conversion systems*. A technology reviews. *Renewable and Sustainable Energy Reviews*, Vol. 51, November 2015, pp. 1288-1305.
<https://doi.org/10.1016/j.rser.2015.06.060>
- Hassanain, N. A. M., & Fletcher, J. E. (2007). *Analysis three- and five-phase permanent magnet machines supplying diode bridge rectifiers for small-scale wind generators*. 2007 International Conference on Power Engineering, Energy and Electrical Drives, 2007, pp. 648-653.
<https://doi.org/10.1109/POWERENG.2007.4380174>
- Parsa, L., Toliyat, H. A., & Goodarzi, A. (2007). *Five-Phase Interior Permanent-Magnet Motors with Low Torque Pulsation*. in *IEEE Transactions on Industry Applications*, Vol. 43, Issue 1, pp. 40-46, Jan.-Feb.2007.
<https://doi.org/10.1109/TIA.2006.887235>
- Reusser, C. A., Kouro, S., & Cardenas, R. (2015). *Dual three-phase PMSG based wind energy conversion system using 9-switch dual converter*. 2015 IEEE Energy Conversion Congress and Exposition (ECCE), 2015, pp. 1021-1022.

- <https://doi.org/10.1109/ECCE.2015.7309800>
11. I. Abdelsalam, G. P. Adam, D. Holliday, and B. W. Williams, "Assessment of a wind energy conversion system based on a six-phase permanent magnet synchronous generator with a twelve-pulse PWM current source converter," 2013 IEEE ECCE Asia Downunder, 2013, pp. 849-854. <https://doi.org/10.1109/ECCE-Asia.2013.6579203>
 12. Mekri, F., Benelghali, S., Benbouzid, M., & Charpentier, J. F. (2011). "A fault-tolerant multiphase permanent magnet generator for marine current turbine applications". 2011 IEEE International Symposium on Industrial Electronics, 2011, pp. 2079-2084, <https://doi.org/10.1109/ISIE.2011.5984481>
 13. Dwari, S., & Parsa, L. (2011). "Fault-Tolerant Control of Five-Phase Permanent-Magnet Motors with Trapezoidal Back EMF". IEEE Transactions on Industrial Electronics, Vol. 58, Issue 2, pp. 476-485, Feb. 2011. <https://doi.org/10.1109/TIE.2010.2045322>
 14. D. Kumar, K. Chatterjee, "A review of conventional and advanced MPPT algorithms for wind energy systems," Renew. Sustain. Energy Rev. Vol. 55, March 2016, pp. 957-970. <https://doi.org/10.1016/j.rser.2015.11.013>.
 15. Errami, Y., Obbadi, A., & Sahnoun, S. (2020). "MPPT Control for Grid Connected Wind Energy Conversion System Based Permanent Magnet Synchronous Generator (PMSG) and Five-Level Neutral Point Clamped Converter". IOP Conference Series: Materials Science and Engineering, Vol. 765, Issue 1, 012042. <https://doi.org/10.1088/1757-899X/765/1/012042>
 16. Putri, R. I., Pujiantara, M., Priyadi, A., Hery, P. M., & Taufik. (2016). "Optimum control strategy of grid connected PMSG wind turbine based on energy storage system". 2016 International Seminar on Intelligent Technology and Its Applications (ISITIA), 2016, pp. 623-628. <https://doi.org/10.1109/ISITIA.2016.7828732>
 17. Ramesh, M., & Jyothsna, T. R. (2016). "A concise review on different aspects of wind energy system". 2016 3rd International Conference on Electrical Energy Systems (ICEES), 2016, pp. 222-227. <https://doi.org/10.1109/ICEES.2016.7510644>
 18. Zhou, J. Z., Ding, H., Fan, S., Zhang, Y., & Gole, A. M. (2014). "Impact of Short-Circuit Ratio and Phase-Locked-Loop Parameters on the Small-Signal Behavior of a VSC-HVDC Converter". IEEE Transactions on Power Delivery, Vol. 29, Issue 5, pp. 2287-2296, Oct. 2014. <https://doi.org/10.1109/TPWRD.2014.2330518>
 19. Hu, L., Xue, F., Qin, Z., Shi, J., Qiao, W., Yang, W., & Yang, T. (2019). "Sliding mode extremum seeking control based on improved invasive weed optimization for MPPT in wind energy conversion system". Applied Energy, Vol. 248, 15 August 2019, pp. 567-575. <https://doi.org/10.1016/j.apenergy.2019.04.073>
 20. Asri, A., Mihoub, Y., Hassaine, S., Logerais, P., & Allaoui, T. (2019). "Intelligent maximum power tracking control of a PMSG wind energy conversion system". Asian Journal of Control, Vol.21, Issue 4, pp. 1980-1990. <https://doi.org/10.1002/asjc.2090>

21. Mousa, H. H. H., Youssef, A.-R., & Mohamed, E. E. M. (2020). "Optimal power extraction control schemes for five-phase PMSG based wind generation systems". Engineering Science and Technology, an International Journal. Vol. 23, Issue 1, February 2020, pp. 144-155. <https://doi.org/10.1016/j.jestch.2019.04.004>
22. Janaszek, M. (2016). "Structures of vector control of n-phase motor drives based on generalized Clarke transformation". Bulletin of the Polish Academy of Sciences Technical Sciences, Vol. 64, Issue (4), pp. 865–872. <https://doi.org/10.1515/bpasts-2016-0094>
23. Hosseyni, A., Trabelsi, R., Mimouni, M. F., & Iqbal, A. (2014). "Vector controlled five-phase permanent magnet synchronous motor drive". 2014 IEEE 23rd International Symposium on Industrial Electronics (ISIE), 2014, pp. 2122-2127. <https://doi.org/10.1109/ISIE.2014.6864945>
24. Amira, L., Tahar, B., & Abdelkrim, M. (2020). "Sliding Mode Control of Doubly-fed Induction Generator in Wind Energy Conversion System". 2020 8th International Conference on Smart Grid (icSmartGrid), 2020, pp. 96-100. <https://doi.org/10.1109/icSmartGrid49881.2020.9144778>
25. MEHEDI, F., NEZLI, L., & MAHMOUDI, M. O. (2018). "Speed Control of Series-Connected Five-Phase Two PMSM using Sliding Mode Control". 2018 International Conference on Electrical Sciences and Technologies in Maghreb (CISTEM), 2018, pp. 1-6. <https://doi.org/10.1109/CISTEM.2018.8613341>
26. Rezkallah, M., Sharma, S. K., Chandra, A., Singh, B., & Rouse, D. R. (2017). "Lyapunov Function and Sliding Mode Control Approach for the Solar-PV Grid Interface System". IEEE Transactions on Industrial Electronics, Vol. 64, Issue 1, pp. 785-795, Jan. 2017. <https://doi.org/10.1109/TIE.2016.2607162>
27. Merabet, A., Labib, L., Ghias, A. M. Y. M., Ghenai, C., & Salameh, T. (2017). "Robust Feedback Linearizing Control with Sliding Mode Compensation for a Grid-Connected Photovoltaic Inverter System Under Unbalanced Grid Voltages". IEEE Journal of Photovoltaics, Vol. 7, Issue3, pp. 828-838, May 2017. <https://doi.org/10.1109/JPHOTOV.2017.2667724>
28. B. Yang, T. Yu, H. Shu, Y. Zhang, J. Chen, Y. Sang, L. Jiang, (2018) "Passivity-based sliding-mode control design for optimal power extraction of a PMSG based variable speed wind turbine", Renew. Energy, Vol. 119, April 2018, pp. 577-589. <https://doi.org/10.1016/j.renene.2017.12.07>
29. Sun, D., Wang, X., Nian, H., & Zhu, Z. Q. (2018). "A Sliding-Mode Direct Power Control Strategy for DFIG Under Both Balanced and Unbalanced Grid Conditions Using Extended Active Power". IEEE Transactions on Power Electronics, Vol. 33, Issue 2, pp. 1313-1322, Feb. 2018. <https://doi.org/10.1109/TPEL.2017.2686980>
30. Xiong, L., Wang, J., Mi, X., & Khan, M. W. (2018). "Fractional Order Sliding Mode Based Direct Power Control of Grid-Connected DFIG". IEEE Transactions on Power Systems, Vol. 33, Issue3, pp. 3087-3096, May 2018. <https://doi.org/10.1109/TPWRS.2017.2761815>
31. Sadeghi, R., Madani, S. M., Ataei, M., Agha Kashkooli, M. R., & Ademi, S. (2018). "Super-Twisting Sliding Mode Direct Power

- Control of a Brushless Doubly Fed Induction Generator". IEEE Transactions on Industrial Electronics, Vol. 65, Issue 11, pp. 9147-9156, Nov. 2018.*
<https://doi.org/10.1109/TIE.2018.2818672>
32. Shtessel, Y., Edwards, C., Fridman, L., & Levant, A. (2014). *"Sliding Mode Control and Observation"*. Springer New York. ISBN: 978-0-8176-4893-0.
<https://doi.org/10.1007/978-0-8176-4893-0>
33. Mousa, H. H. H., Youssef, A.-R., & Mohamed, E. E. M. (2019). *"Variable step size P&O MPPT algorithm for optimal power extraction of multi-phase PMSG based wind generation system"*. International Journal of Electrical Power & Energy Systems, Vol. 108, June 2019, pp. 218-231.
<https://doi.org/10.1016/j.ijepes.2018.12.044>
34. Youssef, Abdel-Raheem & Sayed, Mahmoud & Abe Wahab, M.N. & Shabib, Gaber & Sayed, M. (2015). *"MPPT Control Technique for Direct-Drive Five-Phase PMSG Wind Turbines with Wind Speed Estimation"*. International Journal of Sustainable and Green Energy. Vol. 4, Issue 5, September 2015, pp. 195-205.
<https://doi.org/10.11648/j.ijrse.20150405.14>
35. Toliyat, H. A., Rahimian, M. M., & Lipo, T. A. (n.d.). (1991). *"dq modeling of five phase synchronous reluctance machines including third harmonic of air-gap MMF"*. Conference Record of the 1991 IEEE Industry Applications Society Annual Meeting, 1991, pp. 231-237 vol.1.
<https://doi.org/10.1109/IAS.1991.178160>
36. Moutchou, R., & Abbou, A. (2021). *"Control of grid side converter in wind power based PMSG with PLL method"*. International Journal of Power Electronics and Drive Systems (IJPEDS), Vol 12, Issue 4, pp. 2191- 2200.
<https://doi.org/10.11591/ijped.v12.i4>
37. Nasiri, M., Milimonfared, J., & Fathi, S. H. (2015). *"A review of low-voltage ride-through enhancement methods for permanent magnet synchronous generator based wind turbines"*. Renewable and Sustainable Energy Reviews, Vol. 47, July 2015, pp. 399-415.
<https://doi.org/10.1016/j.rser.2015.03.079>

Appendix – I

Parameters of WECS [33,37]

II. Characteristics of wind turbines

The blade's radius	R = 30.65 m
Density of air	$\rho = 1.255 \text{ kg/m}^3$
TSR optimum	$\lambda = 8.1$
Maximum power	C = 0.48
Coefficient	

II. The five-phase PMSG parameters

Rated power	P = 1.5 MW
Number of pole pairs	n = 40
Stator resistance	$R_s = 3.17 \text{ m}\Omega$
Stator inductance	$L_s = 3.07 \text{ mH}$
Moment of inertia	J = 10000 kg.m ²
Flux linkage	$\psi = 7.0172 \text{ wb}$

III. Parameters for the DC bus and grid

Voltage of dc-link	$V_{dc} = 1150 \text{ V}$
DC-link capacitor	C = 0.003 F
Grid voltage	$V_g = 575 \text{ V}$
Grid frequency	F = 60 Hz
Grid resistance	$R_g = 0.002 \Omega$
Grid inductance	$L_g = 400 \mu\text{H}$

Appendix –II

GSC's PI-controller gains

K_{pvdc}	8
K_{ivdc}	400
K_{piq}	10
K_{iiq}	20
K_{pid}	10
K_{iid}	20

MSC's PI controller gains

K_p	15
K_i	35

MSC's ISMC controller gains

K_p	8
K_i	0.1
ρ_ω	35
K_c	5
K_t	3.5

MSC's TSMC controller gains

r_1	100
r_2	0.8
K_s	30
K_ω	14.8
